Single-particle states in nuclear matter and in finite nuclei

R. Sartor
Institut für Theoretische Physik, Universität Tübingen, 7400 Tübingen, West Germany and Institut de Physique, Université de Liège, Sart Tilman, 4000 Liège 1, Belgium

C. Mahaux
Institut de Physique, Université de Liège, Sart Tilman, 4000 Liège 1, Belgium
(Received 7 November 1979)

The complex single-particle field in nuclear matter is computed in the framework of Brueckner's theory, in the case of the realistic nucleon-nucleon interaction of Hammann and Ho-Kim. The Hartree-Fock, the core polarization, and the correlation contributions are calculated; renormalization corrections are also evaluated. The results are compared with those derived from a dispersion relation approach. Particular attention is paid to the behavior of the effective mass near the Fermi surface, where it presents a narrow enhancement. Following a recent suggestion by Orland and Schaeffer, the nuclear matter results are adapted to finite nuclei by assuming that the relevant variable is the difference between the single-particle energy and the Fermi energy. This yields fair agreement between the strength functions for quasihole states calculated here and those measured from $(e,e'p)$ knockout processes.

[NUCLEAR STRUCTURE Potential energy and width of single-particle states from Hammann–Ho-Kim interaction.]

I. INTRODUCTION

Bethe[1] emphasized that "the most striking feature of finite nuclei is the validity of the shell model. Nuclei can be very well described by assigning quantum numbers to individual nucleons." In the simple case of nuclear matter, the latter sentence amounts to stating that one can associate a well-defined energy to nucleons with a given wavelength. Landau[2-4] explained the success of the shell model by the fact that for small excitation energies the spectrum of an interacting Fermi gas can be described in terms of excitations of nucleons surrounded by their polarization clouds, i.e. of quasiparticles; these move independently in a smooth mean potential, possibly nonlocal. For soft phenomenological nucleon-nucleon interactions, this static potential is usually identified with the Hartree-Fock field, which is represented by graph (IA) in Fig. 1.

The validity of the concept of quasiparticles has been justified theoretically for single-particle states close to the Fermi surface. The empirical success of the optical model shows that this concept is also valid for scattering states.[5] Besides, the quasiparticle model is often used for deeply bound single-particle states, for instance when using a Hartree-Fock description of nuclear ground states. It is of interest to investigate whether this extension is valid. Experimentally, most information in this respect is obtained from $(e,e'p)$ or $(p,2p)$ knockout reactions. Theoretically, one must study whether for a deeply bound state the single-particle strength is still sharply peaked about the single-particle energy. This problem involves the study of the "true" energy dependence of the mean field. The existence of this energy dependence reflects the interaction between quasiparticle states. The dispersion relation (2.6) below, which connects the real and imaginary parts of the mean field, shows that the energy dependence is intimately related to the fact that the mean field is complex. The imaginary part of the field accounts for the spreading of the single-particle strength.

A theoretical investigation of these properties of the mean field implies that one carries the calculation beyond the Hartree-Fock approximation, since the latter is real and static. If one uses a soft phenomenological nucleon-nucleon interaction, the natural way to proceed is to add to the first-order field (IA) the second-order contributions, represented by the "polarization" diagram (IIA) and by the "correlation" graph (IIB).[6] In the case of nuclear matter, the energy dependence of these second-order contributions has recently been investigated by Orland and Schaeffer[7] on the basis of the dispersion relation (2.6). In Ref. 8, we show that part of their discussion is marred by the use of a somewhat arbitrary parametrization of the energy dependence of the imaginary part of the mean field. This led us to perform an explicit evaluation of the real and imaginary parts of graphs (IA), (IIA), and (IIB). More precisely, we have computed the Brueckner-Hartree-Fock approximation, which is rep-

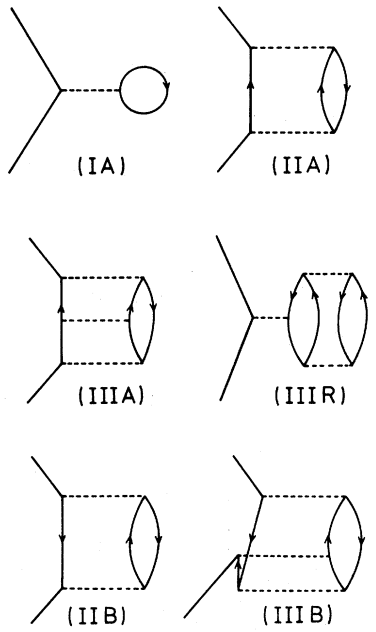

FIG. 1. Graphical representation of the leading terms of the perturbation expansion of the mass operator. Only direct terms are drawn. Graph (IA) is the Hartree-Fock approximation, (IIA) is the polarization graph, and (IIB) the correlation graph. Diagram (IIIR) yields the renormalization of graph (IA).

resented by graph (BHF) in Fig. 2. This is the sum of a series of particle-particle ladders of which graphs (IA), (IIA), and (IIIA) of Fig. 1 are the leading terms. We have also computed the real and the imaginary parts of the graph (CO) of Fig. 2, which is the sum of a series of diagrams of which graphs (IIB) and (IIIB) of Fig. 1 are the leading terms.

The input of our calculation is the nucleon-nucleon interaction of Hammann and Ho-Kim.[9] This interaction is a realistic one since it renders with good accuracy the S, P, and D nucleon-nucleon scattering phase shifts. However, it is in some sense only semirealistic because it has

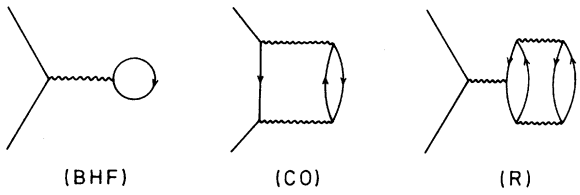

FIG. 2. Graphical representation of some contributions to the low-density expansion of the mass operator. Graph (BHF) represents the Brueckner-Hartree-Fock approximation (CO) shows the correlation contribution. The sum of graphs (BHF) and (R) yields the renormalized Brueckner-Hartree-Fock approximation.

finite rank, i.e., is strongly nonlocal. This influences the nonlocality of the corresponding single-particle mean field. Moreover, the average binding energy per nucleon at normal density as calculated from the Brueckner-Hartree-Fock approximation is larger than the empirical value; we note that the Hartree-Fock approximation yields good agreement with the empirical binding energy. These deficiencies have to be kept in mind when discussing our results. They are overshadowed by the following two features. Firstly, the interaction is sufficiently soft for using a perturbation expansion. Secondly, Brueckner's reaction matrix can be computed faster and more accurately than for a local interaction.

The interaction of Hammann and Ho-Kim has already been used in Refs. 10 and 11 to investigate some properties of bound single-particle states. In the present paper, we take advantage of the two features mentioned above to calculate separately the contributions to the single-particle mean field of specific graphs of the perturbation expansion, and to compare these results with those recently obtained by Orland and Schaeffer[7] who used the dispersion relation (2.6). Moreover, we investigate the shape of the enhancement of the effective mass near the Fermi surface in more detail than was previously possible in the case of the local Reid's hard core interaction.[5] Finally, the comparison between quantities calculated in nuclear matter and empirical data is performed by assuming that the relevant variable that provides a link between the two cases is the difference between the single-particle energy and the Fermi energy. This method is based on a suggestion by Orland and Schaeffer.[7] It yields better agreement between calculated and measured quantities than the approach used in Refs. 10–12, and which consisted in identifying the momentum of a particle in nuclear matter with the average momentum of a single-particle state in a finite nucleus.

A few useful formulas and concepts are briefly recalled in Sec. II. Section III is devoted to the real part of the mean field. In Secs. III A–III C, we successively discuss some properties of the Hartree-Fock approximation, of the core polarization contribution, and of the correlation graph. We pay particular attention to the vicinity of the Fermi surface, where the empirical effective mass is known to be enhanced.[13] The size of the renormalization corrections is evaluated in Sec. III D. Our results are compared with the dispersion approach of Orland and Schaeffer[7] in Sec. III E and with empirical values in Sec. III F.

The imaginary part of the mean field is investi-

gated in Sec. IV, where we compare it with the value used by Orland and Schaeffer, and also with a compilation of empirical data.

In Sec. V, we calculate the strength function of quasihole states, i.e., the distribution of the spread single-particle states. We obtain fair agreement between calculated and measured strength functions by equating in the two cases the difference between the single-particle energy and the Fermi energy. As mentioned above, this method follows a suggestion by Orland and Schaeffer.[7] It presents over that used in Refs. 10–12 the advantages of identifying the main relevant variable, and of compensating part of the deficiencies of the interaction of Hammann and Ho-Kim.

II. BASIC FORMULAS

A. Definitions

The equations and results given in Secs. II–IV refer to infinite nuclear matter with equal number of neutrons and protons. Insofar as possible, we follow the notation of Ref. 5, where proofs or references to the original papers can be found. We denote by ρ the nucleon density and by k_F the Fermi momentum. They are related by

$$\rho = 2(3\pi^2)^{-1} k_F^{\,3} . \tag{2.1}$$

The mass operator

$$\lim_{\eta \to 0} M(k; E - i\eta) = M(k;E) = V(k;E) + iW(k;E) \tag{2.2}$$

depends on k_F. It can be identified with the single-particle field felt by a nucleon with momentum k and energy E. One has $W(k;E) \geq 0$.

Most physical processes can be described in terms of quasiparticles. A quasiparticle with momentum k has a well-defined energy $E(k)$ given by the relation ($\hbar = 1$)

$$E(k) = k^2/2m + V(k;E(k)) . \tag{2.3a}$$

The mean field felt by a quasiparticle with momentum k is the on-shell value of the mass operator:

$$M(k;E(k)) = \tilde{M}(k) = \tilde{V}(k) + i\tilde{W}(k) . \tag{2.4}$$

The Fourier transform $\mathfrak{M}(|\vec{r} - \vec{r}\,'|)$ of $\tilde{M}(k)$ yields a static nonlocal field. Equivalently, one may specify the energy E of a quasiparticle, and determine its momentum $k(E)$ by the energy-momentum relation

$$E = [k(E)]^2/2m + V(k(E);E) . \tag{2.3b}$$

The corresponding mean field is the on-shell value

$$M(k(E);E) = \bar{M}(E) = \bar{V}(E) + i\bar{W}(E) , \tag{2.5}$$

which is a local energy-dependent field.

The fields $\bar{M}(E)$ and $\tilde{M}(k)$ are equivalent in the sense that they yield the same quasiparticle properties. In a finite system, they are phase equivalent since they yield practically the same phase shifts, though the corresponding scattering wave functions are different in the nuclear interior. In nuclear reaction analyses, one normally uses a local energy-dependent optical-model potential which should thus be identified with $\bar{M}(E)$. In bound state calculations, one often uses a nonlocal static shell-model potential (e.g., in a Hartree-Fock model); it should be identified with $\tilde{M}(k)$.

When the nucleon-nucleon interaction has no hard core, the following dispersion relation holds:

$$V(k;E) = M_{(\mathrm{IA})}(k) + \frac{\mathcal{P}}{\pi} \int_{-\infty}^{\infty} \frac{W(k;E')}{E - E'} dE' , \tag{2.6a}$$

where $\mathcal{P}$ denotes a principal value integral. The energy-independent background $M_{(\mathrm{IA})}(k)$ is the Hartree-Fock contribution to the real part of the mean field. In the presence of a hard core repulsion, one must use the subtracted dispersion relation[8]

$$V(k;E) = V(k;E_0) + \frac{E_0 - E}{\pi} \mathcal{P} \int_{-\infty}^{\infty} \frac{W(k;E')}{(E - E')(E_0 - E')} dE' , \tag{2.6b}$$

where E_0 is arbitrary.

B. Perturbation expansion

The nucleon-nucleon potential of Hammann and Ho-Kim[9] is sufficiently soft for using a perturbation expansion in powers of the strength of the interaction. Some contributions are represented in Fig. 1. The first-order term is the Hartree-Fock (HF) approximation

$$M_{(\mathrm{IA})}(k) = M_{\mathrm{HF}}(k) = \sum_{j < k_F} \langle \vec{k}, \vec{j} | v | \vec{k}, \vec{j} \rangle_{\mathcal{A}} . \tag{2.7}$$

Here, v is the nucleon-nucleon potential and $\mathcal{A}$ refers to antisymmetrization. Note that $M_{\mathrm{HF}}(k)$ is real and independent of E.

There exist two second-order terms. They are energy dependent and complex. The "polarization" contribution is represented by graph (IIA); its algebraic expression reads

$$M_{(\mathrm{IIA})}(k;E) = \tfrac{1}{2} \sum_{j < k_F} \sum_{a,b > k_F} \frac{|\langle \vec{k}, \vec{j} | v | \vec{a}, \vec{b} \rangle_{\mathcal{A}}|^2}{E + E(j) - E(a) - E(b) - i\eta} . \tag{2.8}$$

We recall that the function $E(n)$ is defined by the

energy-momentum relation (2.3). The "correlation" contribution is represented by graph (IIB):

$$M_{(\mathrm{IIB})}(k;E)=\tfrac{1}{2}\sum_{l,j<k_F}\sum_{a>k_F}\frac{|\langle\vec{j},\vec{l}\,|v|\vec{k},\vec{a}\rangle_a|^2}{E+E(a)-E(j)-E(l)-i\eta}\,. \tag{2.9}$$

C. Low-density expansion

The sum of the one-hole line graphs (IA), (IIA), (IIIA),... of Fig. 1 yields the Brueckner-Hartree-Fock (BHF) approximation

$$M_{\mathrm{BHF}}(k;E)=\sum_{j<k_F}\langle\vec{k},\vec{j}\,|g[E+E(j)]\,|\vec{k},\vec{j}\rangle_a\,. \tag{2.10}$$

Here, $g[E+E(j)]$ is the reaction matrix. It is the solution of the integral equation

$$g[E+E(j)]=v+v\sum_{a,b>k_F}\frac{|\vec{a},\vec{b}\rangle\langle\vec{a},\vec{b}\,|}{E+E(j)-E(a)-E(b)-i\eta}\times g[E+E(j)]\,. \tag{2.11}$$

The BHF approximation is represented by the graph denoted by (BHF) in Fig. 2.

The sum of the graphs (IIB), (IIIB),... of Fig. 1 yields the diagram labeled (CO) in Fig. 2. It reads

$$M_{(\mathrm{CO})}(k;E)=\tfrac{1}{2}\sum_{l,j<k_F}\sum_{a>k_F}\frac{|\langle\vec{j},\vec{l}\,|g[E(j)+E(l)]\,|\vec{k},\vec{a}\rangle_a|^2}{E+E(a)-E(j)-E(l)-i\eta}\,. \tag{2.12}$$

By analogy with Eq. (2.9), we also call $M_{(\mathrm{CO})}$ a correlation graph.

Graph (IIIR) in Fig. 1 is the progenitor of a series of graphs whose sum is represented by graph (R) in Fig. 2. The sum of graphs (BHF) and (R) yields the "renormalized" Brueckner-Hartree-Fock approximation; it reads

$$M^{\mathrm{R}}_{\mathrm{BHF}}(k;E)=(1-\kappa)M_{\mathrm{BHF}}(k;E)\,. \tag{2.13}$$

Here, $1-\kappa$ denotes the average occupation number in the Fermi sea. In the case of the interaction of Hammann and Ho-Kim one has[10]

$$\kappa\simeq 0.08 \tag{2.14}$$

for $k_F=1.17$ fm^{-1} as well as for $k_F=1.36$ fm^{-1}. Engelbrecht and Weidenmüller[14] have argued that the correlation contribution (2.12) can also be renormalized, with the result

$$M^{\mathrm{R}}_{(\mathrm{CO})}(k;E)=(1-\kappa)^2M_{(\mathrm{CO})}(k;E)\,. \tag{2.15}$$

Unless otherwise specified, the single-particle energy $E(k)$ will henceforth be approximated by its BHF value ($\hbar=1$)

$$E(k)=k^2/2m+V_{\mathrm{BHF}}(k;E(k))\,. \tag{2.16a}$$

The Fermi energy E_F will be identified with $E(k_F)$:

$$E_F=E(k_F)\,. \tag{2.17}$$

Occasionally, we shall also consider the second-order approximation

$$E^{(2)}(k)=k^2/2m+V_{\mathrm{BHF}}(k;E(k))+V_{(\mathrm{CO})}(k;E(k))\,, \tag{2.16b}$$

and the renormalized second-order approximation

$$E^{\mathrm{R}}(k)=k^2/2m+V^{\mathrm{R}}_{\mathrm{BHF}}(k;E(k))+V^{\mathrm{R}}_{(\mathrm{CO})}(k;E(k))\,. \tag{2.18}$$

III. REAL PART OF THE MEAN FIELD

A. Hartree-Fock approximation

The short dashes in Fig. 3 represent the value of the Hartree-Fock approximation

$$\tilde{V}_{(\mathrm{IA})}(k)=\overline{V}_{(\mathrm{IA})}(E(k)) \tag{3.1}$$

to the mean field felt by a quasiparticle with momentum k [and thus with energy $E(k)$]. At the Fermi surface, one has $V_{(\mathrm{IA})}(k)=-50$ MeV. The empirical value of the Fermi energy is

$$\epsilon_F=-16\ \mathrm{MeV} \tag{3.2}$$

for $k_F=1.36$ fm^{-1}. This yields the following depth for the quasiparticle potential at the Fermi surface and for $k_F=1.36$ fm^{-1}:

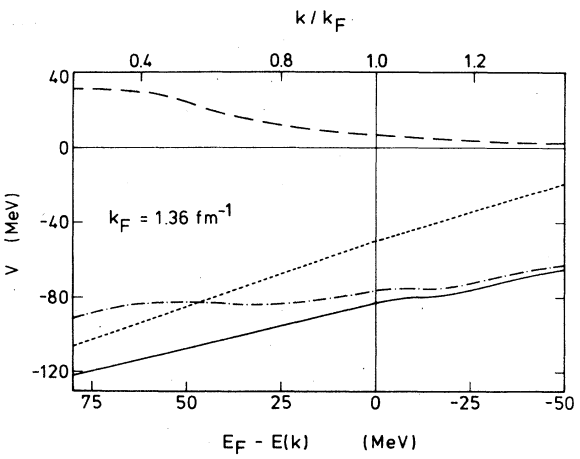

FIG. 3. Dependence upon k/k_F (upper scale) and upon $E_F-E(k)$ (lower scale) of various contributions to the real part $V(k;E(k))$ of the quasiparticle field, in the case of the interaction of Hammann and Ho-Kim and for $k_F=1.36$ fm^{-1}. The short dashes represent the Hartree-Fock approximation. The full curve shows the BHF approximation. The long dashes give the correlation contribution. The dash and dots represent the sum of the correlation contribution and of the BHF approximation.

$$V(k_F) = -16 - k_F^2/2m = -54.4 \text{ MeV} . \quad (3.3)$$

This is in fair agreement with the Hartree-Fock value. However, we shall see in the next sections that this agreement between theory and experiment is spoiled when higher-order contributions are taken into account.

The dependence of the mean field upon the quasiparticle energy is characterized by the effective mass $m^*(E)$, which is defined by the equivalent relations

$$m^*(E)/m = 1 - \frac{d}{dE}\bar{V}(E) \quad (3.4a)$$

$$= \left[1 + \frac{m}{k}\frac{d}{dk}\tilde{V}(k)\right]^{-1} . \quad (3.4b)$$

Figure 3 shows that the dependence of $\bar{V}_{(IA)}(E)$ upon E is approximately linear. Hence, the effective mass is almost independent of E in the Hartree-Fock approximation. In the case of the Hammann–Ho-Kim interaction and for $k_F = 1.36$ fm^{-1}, the dotted curve in Fig. 3 yields

$$m^*_{(IA)}(E)/m \approx 0.35 \text{ for } |E - E_F| < 50 \text{ MeV} . \quad (3.5)$$

The property that the Hartree-Fock approximation yields an effective mass which is almost independent of energy is largely independent of the nature of the nucleon-nucleon interaction. It reflects the static nature of the Hartree-Fock field, i.e., the fact that $V_{(IA)}(k)$ is independent of E. In the case of the interaction of Hammann and Ho-Kim, the value of the effective mass calculated in the Hartree-Fock approximation is particularly small. This is due to the strongly nonlocal nature of the interaction, which has finite rank. This should be kept in mind when comparing the calculated effective mass with the empirical value.

Empirical data will be compared with theory in Sec. III F. Here, we only summarize some of their main features. In the domain $E - E_F > 20$ MeV, the effective mass can be determined accurately by investigating the energy dependence of the real part of the optical-model potential. This yields

$$m^*(E)/m = 0.68 \text{ for } E - E_F > 20 \text{ MeV} . \quad (3.6)$$

Information on the effective mass near the Fermi energy can be obtained from the density of weakly bound single-particle states. One finds

$$m^*(E)/m \approx 1 \text{ for } |E - E_F| < 10 \text{ MeV} . \quad (3.7)$$

The value of the effective mass at the bottom of the Fermi sea is poorly known, because the corresponding single-particle states are widely spread. It appears that

$$m^*(E)/m \approx 0.7 \text{ for } E - E_F < -20 \text{ MeV} . \quad (3.8)$$

Equations (3.6)–(3.8) show that the empirical effective mass is not independent of energy; it has a maximum near the Fermi surface. It has recently been pointed out that this local enhancement should be taken into account when investigating, e.g., the root mean square radius of valence orbits,[15-18] the empirical value of the Landau parameters,[19] the nuclear gyromagnetic ratios,[20] the gravitational collapse of stars,[21] etc. Hence a detailed theoretical investigation of this enhancement is fully justified. Since it is not present in the Hartree-Fock approximation, it requires the investigation of higher-order contributions.

B. Polarization graph

The BHF approximation $V_{BHF}(k;E(k))$ to the real part of the quasiparticle field is represented by the full curve in Fig. 3, for $k_F = 1.36$ fm^{-1}. At $k = k_F$, one has

$$\tilde{V}_{BHF}(k_F) = -83 \text{ MeV} ; \quad (3.9)$$

the corresponding approximation to the Fermi energy is

$$E(k_F) = -44.6 \text{ MeV} . \quad (3.10)$$

These numbers are much larger, in absolute magnitude, than the empirical values given by Eqs. (3.3) and (3.2). This shows that the interaction of Hammann and Ho-Kim is on the average too attractive; we shall have to correct for this when comparing calculated and measured single-particle energies and widths.

The matrix elements of the reaction matrix g are also larger in absolute magnitude than those of bare nucleon-nucleon interaction v, with a typical ratio

$$\langle g \rangle / \langle v \rangle \approx 83/50 = 1.66 \quad (3.11)$$

for $k_F = 1.36$ fm^{-1}. This shows that the convergence rate of the perturbation expansion is fairly slow. For the simplicity of the discussion, we shall nevertheless assume that the BHF field is well approximated by the sum of graphs (IA) and (IIA) in Fig. 1:

$$V_{BHF}(k;E) \approx V_{(IA)}(k) + V_{(IIA)}(k;E) . \quad (3.12)$$

Then, the on-shell quantity

$$V_{(IIA)}(k;E(k)) = \tilde{V}_{(IIA)}(k) = \bar{V}_{(IIA)}(E(k)) \quad (3.13)$$

of the polarization graph is given by the difference between the ordinates of the full and dotted curves in Fig. 3. The resulting value of expression (3.13) is represented by the short dashes in Fig. 4. The attractive nature of $\tilde{V}_{(IIA)}(k)$ for $k \leq k_F$ directly de-

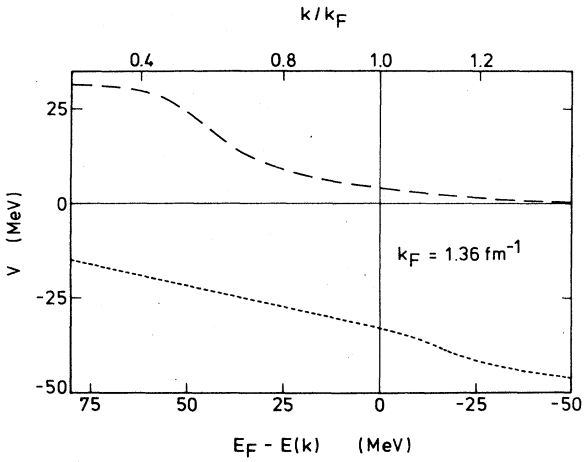

FIG. 4. Dependence upon k/k_F (upper scale) and upon the difference $E_F - E(k)$ (lower scale of the contributions of the polarization graph (short dashes) and of the correlation graph (long dashes) to the potential energy of a quasiparticle, in the case of the interaction of Hammann and Ho-Kim and for $k_F = 1.36$ fm^{-1}.

rives from Eq. (2.8). Equivalently, it can be understood on the basis of the dispersion relation

$$V_{(\mathrm{IIA})}(k;E) = \pi^{-1}\mathcal{P}\int_{E_F}^{\infty} \frac{W_{(\mathrm{IIA})}(k;E')}{E-E'}\,dE', \tag{3.14}$$

and of the fact that

$$W_{(\mathrm{IIA})}(k;E') = 0 \text{ for } E' < E_F, \tag{3.15a}$$

$$W_{(\mathrm{IIA})}(k;E') > 0 \text{ for } E' > E_F. \tag{3.15b}$$

The dependence of $\tilde{V}_{(\mathrm{IIA})}(k)$ upon k can also be characterized by an effective mass, namely

$$m^*_{(\mathrm{IIA})}(E)/m = 1 - \frac{d}{dE}\overline{V}_{(\mathrm{IIA})}(E) \tag{3.16a}$$

$$= \left[1 + \frac{m}{k}\frac{d}{dk}\tilde{V}_{(\mathrm{IIA})}(k)\right]^{-1}. \tag{3.16b}$$

The value of $m^*_{(\mathrm{IIA})}$ is influenced by the dependence of $V_{(\mathrm{IIA})}(k;E)$ upon k on the one hand, and upon E on the other hand. This is exhibited by the following identities, which are also valid for indexed quantities:

$$\frac{m^*(E)}{m} = \frac{\overline{m}(E)}{m}\,\frac{\overline{m}(E)}{m}, \tag{3.17}$$

where the E mass $m(E)$ is defined by

$$\overline{m}(E(k))/m = \left[1 - \frac{\partial}{\partial E}V(k;E)\right]_{E=E(k)}, \tag{3.18}$$

while the k mass $\tilde{m}(E)$ is given by

$$\tilde{m}(E(k))/m = \left[1 + \frac{m}{k}\frac{\partial}{\partial k}V(k;E)\right]^{-1}_{E=E(k)}. \tag{3.19}$$

We first discuss the dependence of $\overline{m}_{(\mathrm{IIA})}(E)$ upon E. Equation (3.12) shows that

$$\overline{m}_{\mathrm{BHF}}(E) = \overline{m}_{(\mathrm{IIA})}(E). \tag{3.20}$$

The quantity $\overline{m}_{\mathrm{BHF}}(E)$ is represented by the long dashes in Figs. 5 and 6, for $k_F = 1.36$ fm^{-1} and 1.18 fm^{-1}, respectively. In the domain $E < E_F$, the inequalities

$$\overline{m}_{\mathrm{BHF}}(E) > m, \quad \frac{d}{dE}[\overline{m}_{\mathrm{BHF}}(E)] > 0 \tag{3.21}$$

directly follow from the dispersion relation (3.14), from which one can also find that

$$\left(\frac{d}{dE}[\overline{m}_{\mathrm{BHF}}(E)]\right)_{E=E_F} = +\infty, \tag{3.22}$$

independently of the nature of the nucleon-nucleon interaction. The fact that $\overline{m}_{\mathrm{BHF}}(E)$ becomes equal to the bare mass m at some energy $E_m > E_F$ is also a rather general feature, valid for all interactions for which the dispersion relation (3.14) holds, i.e., in the absence of a hard core. It follows from the fact that $W_{(\mathrm{IIA})}(k;E')$ vanishes for $E' < E_F$ and for $E' \to \infty$. The value of E_m depends on the nature of the interaction. It would be of interest to clarify what are the main properties of the interaction that determine the value of E_m. In the case of the potential of Hammann and Ho-Kim, Figs. 5 and 6 show that $E_m - E_F \approx 30$ MeV. This implies that the width of the peak of $\overline{m}_{\mathrm{BHF}}(E)$ is about 15 MeV.

The results obtained here are similar to those presented in Ref. 5 in the case of Reid's hard core potential. They are more detailed, because the g matrix can be computed more accurately for the interaction of Hammann and Ho-Kim, hence the interest of the present study. We note that the value of $m/\overline{m}_{\mathrm{BHF}}(E_F)$ calculated here is close to the spectroscopic factors recently computed by Birbrair, Alkhazov, Lapina, and Sadovnika[22] and by Bernard and Van Giai[23] for single-particle levels close to the Fermi surface in ^{208}Pb.

The value of the BHF approximation to the k mass (3.19) is represented by the short dashes in Figs. 6 and 7. At the Fermi surface, one has

$$\tilde{m}_{\mathrm{BHF}}(E_F)/m = 0.36 \tag{3.23}$$

for $k_F = 1.36$ fm^{-1}. This is very close to the value of $m^*_{(\mathrm{IA})}(E_F)/m = \tilde{m}_{(\mathrm{IA})}(E_F)/m$ given by Eq. (3.5). Hence the dependence of $V_{(\mathrm{IA})}(k;E)$ upon k is much smaller than that of $V_{(\mathrm{IIA})}(k)$. This result supports the accuracy of the approximation recently made by Bernard and Nguyen Van Giai,[23] who neglected the dependence upon k of the polarization term (IIA). The value of $\tilde{m}_{\mathrm{BHF}}(E)$ calculated here is approximately 20% smaller than that derived from

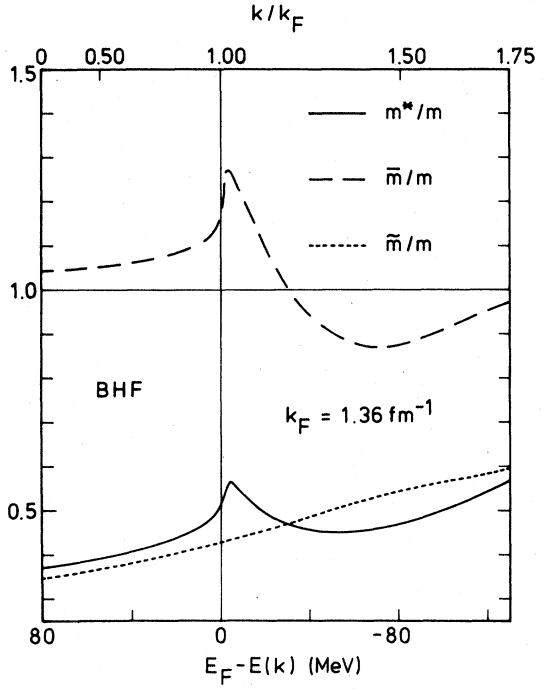

FIG. 5. Dependence upon k/k_F (upper scale) and upon the difference $E_F - E(k)$ (lower scale) of the E mass (long dashes), of the k mass (short dashes), and of the effective mass (full curve), measured in units of the bare mass and evaluated in the framework of the BHF approximation from the interaction of Hammann and Ho-Kim. The value of the Fermi momentum is $k_F = 1.36$ fm^{-1}.

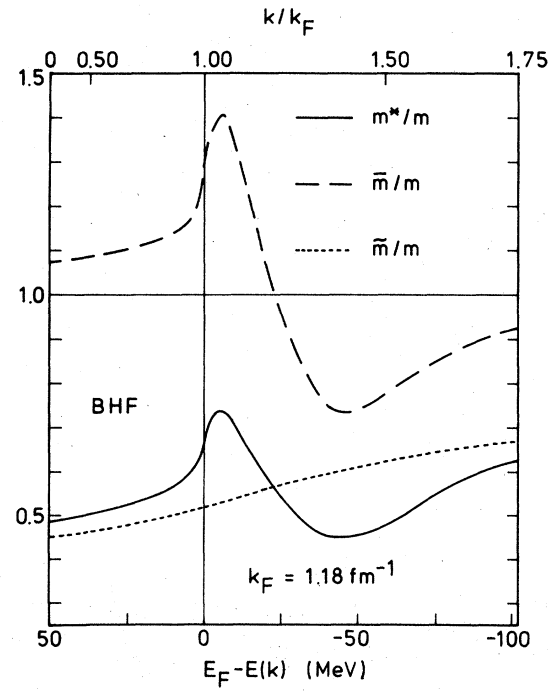

FIG. 6. Same as Fig. 5, for $k_F = 1.18$ fm^{-1}.

Reid's hard core interaction. We argued in Sec. III A that this is mainly due to the strongly nonlocal character of the interaction of Hammann and Ho-Kim.

The BHF approximation of the effective mass is obtained from the Eq. (3.17):

$$\frac{m^*_{\mathrm{BHF}}(E)}{m} = \frac{\bar{m}_{\mathrm{BHF}}(E)}{m}\,\frac{\tilde{m}_{\mathrm{BHF}}(E)}{m}. \tag{3.24}$$

The value of $m^*_{\mathrm{BHF}}(E)/m$ is represented by the full curves in Figs. 5 and 6. The enhancement that it displays near the Fermi surface reflects that of $\bar{m}_{\mathrm{BHF}}(E)$. This feature is in qualitative agreement with the empirical evidence summarized by Eqs. (3.6)–(3.8). However, the calculated value of $m^*_{\mathrm{BHF}}(E)$ is too small for all $E(k)$. This is mainly due to the fact that $\tilde{m}_{\mathrm{BHF}}(E)$ is too small in the case of the interaction of Hammann and Ho-Kim.

The fact that the enhancement of $\bar{m}_{\mathrm{BHF}}(E)$ is located near the Fermi surface must be ascribed to the Pauli principle. This is confirmed by the fact that the enhancement also exists in the case of the hard sphere dilute Fermi gas,[8] in which the shape of $\bar{m}(E)$ is entirely determined by the available phase space for two-particle–one-hole or two-hole–one-particle excitations. The long dashes in Fig. 7 show the value of $\bar{m}_{\mathrm{BHF}}(E)$ in the

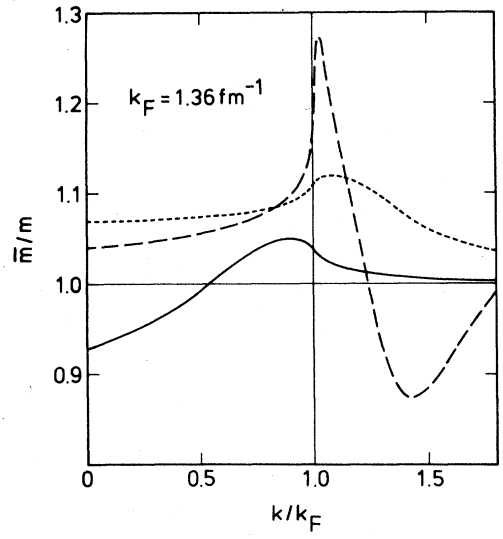

FIG. 7. The long dashes represent the dependence upon k/k_F of $\bar{m}_{\mathrm{BHF}}/m \approx \bar{m}_{(\mathrm{IIA})}/m$ in the case of the interaction of Hammann and Ho-Kim and for $k_F = 1.36$ fm^{-1}. The other curves correspond to the value that $\bar{m}/m$ would take in a hard sphere dilute Fermi gas if one would take into account either the analog of the polarization graph (IIA) (short dashes) or the analog of the correlation graph (IIB) (full curves) (Ref. 8). The hard sphere radius has been adjusted to yield the same average depletion of the Fermi sea for the two interactions.

case of the interaction of Hammann and Ho-Kim. The short dashes correspond to the hard sphere dilute Fermi gas,[8] in which the parameter ($k_F c = 0.426$) has been adjusted in such a way as to yield the same average occupation number below the Fermi surface in the correlated ground state as in the case of the interaction of Hammann and Ho-Kim. Here, c refers to the hard sphere radius. The difference between the shape of $\bar{m}_{\mathrm{BHF}}(E)$ for the two interactions is quite striking. It exhibits the fact that the narrowness of the enhancement peak is largely determined by the long-range part of the nucleon-nucleon interaction.

For $k_F = 1.36$ fm^{-1}, the effective mass as calculated in the Brueckner-Hartree-Fock approximation decreases by 15% when $E(k) - E_F$ increases from 5 to 25 MeV. The enhancement is more pronounced at low density: For $k_F = 1.18$ fm^{-1}, the effective mass decreases by 40% when $E(k) - E_F$ increases from 5 to 25 MeV. Although the variation of m^* is impressive, its influence on the dependence of $V(k;E(k))$ upon $E(k)$ is barely visible in Figs. 3 and 4. In Fig. 4, the enhancement corresponds to the feature that the slope of $V_{(\mathrm{IIA})}(k;E(k))$ (short dashes) is steeper in the energy interval $0 > E_F - E(k) > -25$ MeV than elsewhere. Correspondingly, the single-particle level density is increased in this energy interval, since it is proportional to the product (km^*).[5] We emphasize that this effect is due to the *variation* of the slope of $V_{(\mathrm{IIA})}(k;E(k))$. If the dependence of this quantity upon $E(k)$ could be approximated by a linear law, the polarization graph would increase the Hartree-Fock single-particle level density by the same amount for all energies.

C. Correlation graph

The expression of the correlation graph (CO) in Fig. 2 is given by Eq. (2.12). Its formal similarity with Eq. (2.9) also justifies our use of the expression "correlation graph" for diagram (IIB) in Fig. 1. However, Eq. (3.11) shows that these two graphs are not equal and that their ratio is approximately given by

$$\frac{M_{(\mathrm{CO})}(k;E)}{M_{(\mathrm{IIB})}(k;E)} \approx (1.66)^2 = 2.75 . \tag{3.25}$$

The on-shell value $V_{(\mathrm{CO})}(k;E(k))$ of the correlation graph in the case of the interaction of Hammann and Ho-Kim has been calculated in Refs. 10 and 11. It is represented by the long dashes in Fig. 4. When added to the BHF approximation, it yields the dash and dots in Fig. 3. The corresponding value of the Fermi momentum is

$$E_F^{(2)} = E_F + V_{(\mathrm{CO})}(k_F;E(k_F)) = -37.6 \text{ MeV} .$$

The accuracy of the calculated value of $V_{(\mathrm{CO})}(k;E(k))$ is unfortunately not sufficient to reliably evaluate its derivative, i.e., its influence on the value of the effective mass, nor *a fortiori* its second derivative, i.e., its influence on the energy dependence of the effective mass. From the dispersion relation

$$V_{(\mathrm{CO})}(k;E) = \pi^{-1} \mathcal{P} \int_{-\infty}^{E_F} \frac{W_{(\mathrm{CO})}(k;E')}{E - E'} dE' , \tag{3.26}$$

and from the asymptotic behavior for E' close to E_F

$$W_{(\mathrm{CO})}(k;E') \sim (E' - E_F)^2 \tag{3.27}$$

for $k < 3k_F$.[11] It can easily be checked that

$$W_{(\mathrm{CO})}(k;E_F + 0) > 0 , \tag{3.28}$$

$$[\partial V_{(\mathrm{CO})}(k;E)/\partial E]_{E>E_F} < 0 , \tag{3.29}$$

$$[\partial^2 V_{(\mathrm{CO})}(k;E)/\partial^2 E]_{E=E_F+0} = \infty . \tag{3.30}$$

Inequality (3.29) shows that above the Fermi surface the correlation graph increases the value of the effective mass, as compared to the BHF approximation. The singularities (3.22) and (3.30) cancel one another; the quantity $d\bar{m}(E)/dE$ is therefore finite at $E = E_F$. The hard sphere dilute Fermi gas model suggests that the contribution of the correlation graph to the effective mass essentially amounts to symmetrizing the BHF enhancement peak about E_F, and to increasing its maximum value by about 20%. In the present case, these rough estimates indicate that the enhancement peak of $m^*(E)$ should be almost symmetric about E_F, and that its width at half maximum is approximately equal to 40 MeV. The maximum values would be approximately equal to $m^*(E_F)/m \approx 0.7$ for $k_F = 1.36$ fm^{-1}, and $m^*(E_F)/m \approx 0.9$ for $k_F = 1.18$ fm^{-1}. These are likely to be underestimates of the physical reality, since the k mass $\tilde{m}$ is anomalously small in the case of the interaction of Hammann and Ho-Kim.

D. Renormalization corrections

The sum of the graphs (BHF) and (R) in Fig. 2 yields the renormalized BHF approximation (2.13). In Fig. 8, we plot for $k_F = 1.36$ fm^{-1} the renormalized quantities $(1 - \kappa)\, V_{\mathrm{HF}}(k)$, $V^{\mathrm{R}}_{\mathrm{BHF}}(k;E(k))$, $V^{\mathrm{R}}_{(\mathrm{CO})}(k;E(k))$, and $V^{\mathrm{R}}_{\mathrm{BHF}}(k;E(k)) + V^{\mathrm{R}}_{(\mathrm{CO})}(k;E(k))$ versus the difference $E^{\mathrm{R}}_F - E^{\mathrm{R}}(k)$, with

$$E^{\mathrm{R}}_F = E^{\mathrm{R}}(k_F) = -49.5 \text{ MeV} . \tag{3.31}$$

As expected from the smallness of κ [Eq. (2.14)], the curves shown in Fig. 8 are quite similar to those which appear in Fig. 3. The main origin of the differences is that the renormalized single-particle energy $E^{\mathrm{R}}(k)$ contains the contribu-

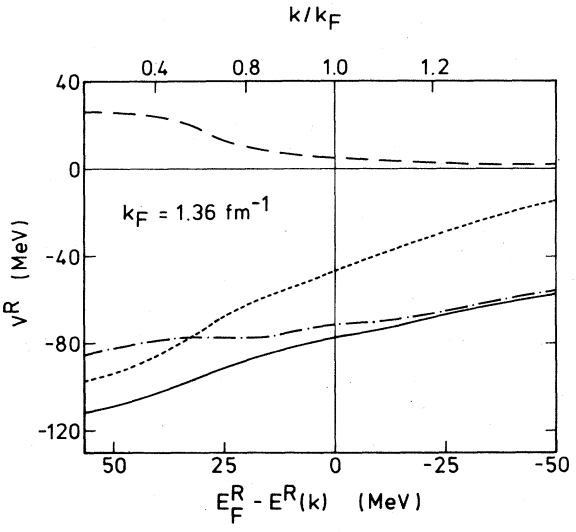

FIG. 8. Dependence upon the difference $E_F^R - E^R(k)$ of the renormalized quantities $(1-\kappa)\, V_{HF}(k)$ (short dashes), $V^R_{BHF}(k; E(k))$ (full curve), $V^R_{(CO)}(k, E(k))$ (long dashes), and $V^R_{BHF}(k; E(k)) + V^R_{(CO)}(k; E(k))$ (dash and dots), for $k_F = 1.36$ fm^{-1} and in the case of the interaction of Hammann and Ho-Kim.

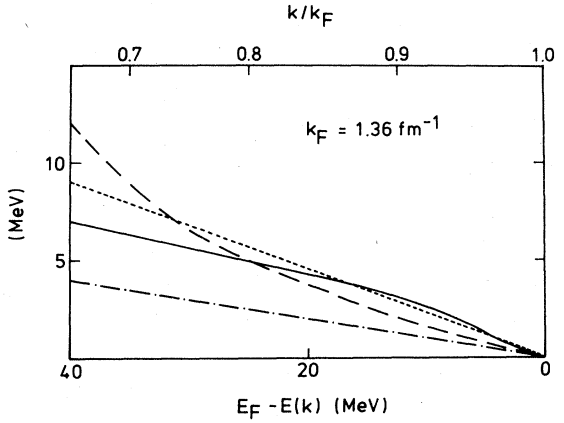

FIG. 9. The quantities (3.32a) and (3.33a) as evaluated by Orland and Schaeffer (Ref. 7) are represented by the full curve and the dash and dots, respectively. The short dashes and the long dashes show the value of (3.32b) and of (3.33b), respectively, for $k_F = 1.36$ fm^{-1} and in the case of the interaction of Hammann and Ho-Kim.

tion of the (renormalized) correlation graph; see Eq. (2.18). In particular, this is responsible for the steep rise of $(1-\kappa)\, V_{HF}$ for $E_F^R - E^R(k) \approx 30$ MeV.

E. Comparision with a dispersion relation approach

Orland and Schaeffer[7] recently evaluated the quantities

$$V_{(IIA)}(k;E) - V_{(IIA)}(k;E_F)\,, \tag{3.32a}$$

and

$$V_{(IIB)}(k;E) - V_{(IIB)}(k;E_F)\,. \tag{3.33a}$$

They used the subtracted dispersion relation (2.6b); see also Eqs. (3.14) and (3.26) where they inserted for $W(k;E')$ algebraic expressions suggested by the hard sphere dilute Fermi gas model. In Fig. 9, we compare their results with the quantities

$$V_{(IIA)}(k;E(k)) - V_{(IIA)}(k_F;E_F)\,, \tag{3.32b}$$

$$V_{(CO)}(k;E(k)) - V_{(CO)}(k_F;E_F)\,, \tag{3.33b}$$

as calculated here from the interaction of Hammann and Ho-Kim. This comparison is legitimate, since Orland and Schaeffer neglected the dependence upon k of the quantities (3.32a) and (3.33a). The overall agreement between the two approaches is fair, despite the fact that both of them suffer from weaknesses. These mainly consist in the parametric expression of $W(k;E')$ used by Orland and Schaeffer on the one hand,[8] and in the finite rank nature of the interaction of Hammann and Ho-Kim on the other hand.

F. Comparison with empirical values

The comparison between our calculated depths and empirical depths can only bear on their energy dependence, since the interaction of Hammann and Ho-Kim yields too much attraction. Accordingly, we shall add to the calculated value of the depth a constant equal to

$$\Delta_{BHF} = \epsilon_F - E_F = 28.6 \text{ MeV} \tag{3.34}$$

in the case of the BHF approximation, and to

$$\Delta_{BHF}{}^{(2)} = \epsilon_F - E_F{}^{(2)} = 21.6 \text{ MeV} \tag{3.35}$$

in the case of the sum of the BHF and of the correlation graphs. One should also keep in mind that the empirical depth depends on the geometry adopted for the mean field, and that moreover the interaction of Hammann and Ho-Kim yields a too large value for the nonlocality range. Despite these reservations, a comparison between calculated and empirical depths is useful, in particular, since it offers an opportunity to show to what extent the experimental data indeed exhibit that the effective mass is enhanced near the Fermi surface.

Bear and Hodgson[24] recently fitted the centroid energies of bound single-particle states with a shell-model potential well whose Woods-Saxon geometry was kept fixed, but whose depth was adjusted in order to reproduce each centroid energy. The resulting empirical depths are represented by open dots (protons) and by crosses (neutrons) in Figs. 10 and 11. The vertical bars

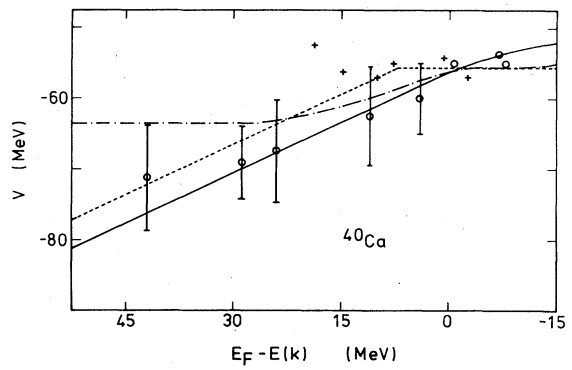

FIG. 10. The dots represent the depth of a Woods-Saxon potential which reproduces the experimental single-particle centroid energy $E(k)$, in the case of ^{40}Ca (Ref. 24). We took $E_F = -8$ MeV. The short dashes show the trend indicated by Bear and Hodgson (Ref. 24). The full curve is the BHF approximation (plus $\Delta_{BHF} = 28.6$ MeV) in the case of nuclear matter with $k_F = 1.36$ fm^{-1} and of the interaction of Hammann and Ho-Kim. The dash and dots correspond to the sum of the BHF approximation and of the correlation term, plus $\Delta^{(2)}_{BHF} = 21.6$ MeV.

indicate the size of the width of the single-particle states. Bear and Hodgson argued that these results suggest the existence of a plateau near the Fermi surface; they accordingly represented this trend by the short dashes, which follow two straight lines. The full curve represents the calculated BHF mean field, plus $\Delta_{BHF} = 28.6$ MeV. The dash and dots corresponds to the sum of the BHF field and of the correlation graph, plus 21.6 MeV.

The overall agreement between calculated and empirical energy dependence is fair. However, several difficulties should be mentioned. Firstly, the empirical depths for proton single-particle states do not exhibit a plateau near the Fermi surface: it is only by combining proton and neutron data that this trend appears. Secondly, the trend is rendered somewhat hazy by the large

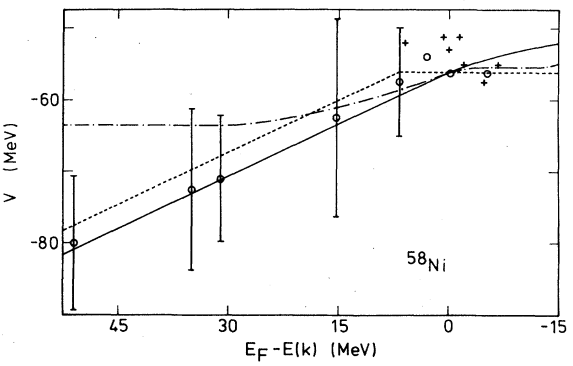

FIG. 11. Same as Fig. 10, in the case of ^{58}Ni.

width of the bound single-particle states. Finally, the energies of the single-particle states close to the Fermi surface are particularly sensitive to the nature of the low-lying core excitations in the case of light and medium-light nuclei. Accordingly, one would expect that the existence of a plateau in the energy dependence of the potential depth should be better exhibited in the case of a heavy nucleus and in the framework of a study that encompasses scattering states. In the case of ^{208}Pb, for instance, the experimental single-particle levels close to the Fermi surface are well reproduced by a static and local Woods-Saxon potential ($m^* = m$). The elastic scattering data require $m^* = 0.7$ m for $E > 20$ MeV.[25] Thus, the combination of bound and scattering data clearly shows that m^* is larger near the Fermi surface than at positive energy. The Skyrme-III interaction ($m^*_{HF} = 0.75$) yields a satisfactory agreement between the Hartree-Fock approximation and bulk nuclear properties; it is thus probably reliable for most bound single-particle states. However, it yields a too small single-particle level density near the Fermi surface.[26] These features suggest that the enhancement of the empirical effective mass is local.

Giannini, Ricco, and Zucchiatti[27] have recently rendered the energies of bound single-particle states and nucleon elastic scattering data for nuclei ranging from C to Sn. The dots in Fig. 12 represent the corresponding empirical depths. We note that in this compilation, the existence of a plateau near $E(k) = E_F$ is better pronounced than in Figs. 10 and 11, owing to the availability of positive energies $E(k)$. As in Figs. 10 and 11, the full curve and the dash and dots correspond

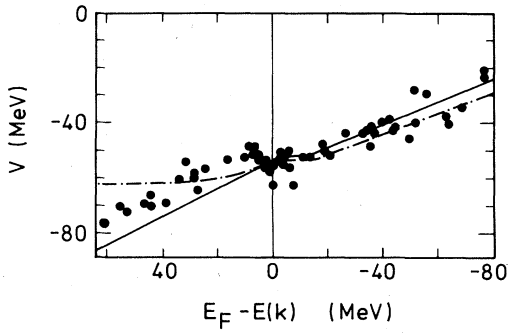

FIG. 12. The dots represent the depth of a Woods-Saxon potential which fits bound single-particle centroid energies [$E(k) < 0$] or elastic scattering data [$E(k) > 0$] (Ref. 27). We took $E_F = -8$ MeV. The full curve is the BHF approximation plus $\Delta_{BHF} = 28.6$ MeV, for nuclear matter with $k_F = 1.36$ fm^{-1} and for the interaction of Hammann and Ho-Kim. The dash and dots correspond to the sum of the Brueckner-Hartree-Fock approximation and of the correlation term, plus $\Delta^{(2)}_{BHF} = 21.6$ MeV.

to the BHF and to the BHF + correlation graph approximation, respectively, including the shifts Δ_{BHF} and $\Delta_{\mathrm{BHF}}^{(\mathrm{CO})}$. The comparison with the data indicates that the calculated enhancement of m^* is somewhat too narrow, and that it should, moreover, be centered on E_F rather than somewhat above E_F. As we discussed in Sec. III C, the hard sphere dilute Fermi gas model suggests that these deficiencies would be largely corrected by a better evaluation of the value of the correlation graph in the vicinity of the Fermi surface.

G. Discussion

There exists experimental evidence that the energy dependence of the depth of the single-particle potential is weaker near the Fermi energy than elsewhere. This corresponds to a local enhancement of the effective mass. This cannot be obtained in the framework of a static description like the Hartree-Fock approximation. One must introduce the dynamics of the shell model by taking into account the coupling of the single-particle states to core excitations, and also the blocking of ground state correlations due to the existence of a valence nucleon. The results presented here confirm and extend the conclusions that had been reached in Ref. 5 from the investigation of the Brueckner-Hartree-Fock calculations in the case of Reid's hard core nucleon-nucleon interaction.

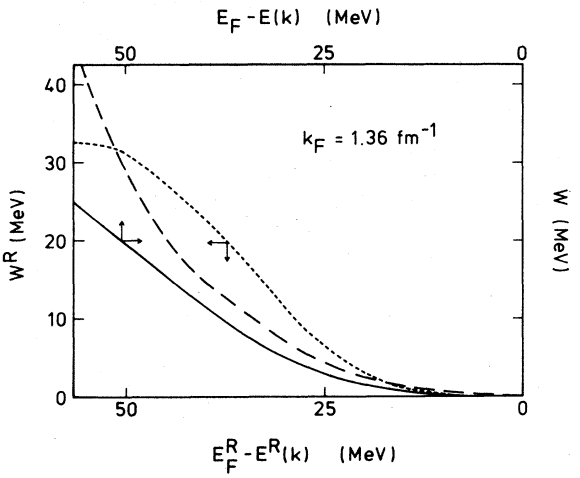

FIG. 13. The full curve (right-hand scale) represents the dependence upon $E_F - E(k)$ (upper scale of the imaginary part of the quasiparticle mean field as calculated for $k_F = 1.36$ fm^{-1} from the interaction of Hammann and Ho-Kim and in the framework of the BHF approximation. The dashed curve (left-hand scale) corresponds to the dependence of the renormalized second-order approximation, Eq. (4.3), upon the energy distance to the Fermi energy as calculated from Eq. (2.18). The long dashes show the result obtained by Orland and Schaeffer (Ref. 7).

One may wonder whether the finiteness of nuclei strongly influences the local enhancement of the effective mass. Hamamoto and Siemens[28] evaluated the increase of the single-particle level density near the Fermi surface of ^{208}Pb in the framework of a particle-vibration coupling model. They found an enhancement which saturates only very slowly with increasing excitation energy of the vibrations. Thus, it appears rather unlikely that the particle-vibration coupling leads to an increase of m^* that would be confined near the Fermi energy. This suggests that the local enhancement of m^* is mainly due to the coupling of single-particle states to one particle-one hole excitations. This is in keeping with the finding that the local enhancement of m^* exists in the limit $A \to \infty$, i.e., for infinite nuclear matter.[5] We note that the effect of the particle vibration is $O(A^{-2/3})$ while the shell spacing in the independent particle approximation is $O(A^{-1/3})$.[28] Hence, the effect of the particle-vibration coupling vanishes in the limit $A \to \infty$, as expected from the surface nature of the vibrations.

IV. IMAGINARY PART OF THE MEAN FIELD

A. Numerical results

The imaginary part of the mean field felt by a quasiparticle with energy $E(k)$ is given by

$$W(E(k)) = W(k; E(k)). \tag{4.1}$$

We shall see in Sec. V that in first approximation the corresponding width of the quasiparticle state is given by

$$\Gamma(E(k)) = 2\bar{W}(E(k)). \tag{4.2}$$

We calculated this quantity from the interaction of Hammann and Ho-Kim. The solid line in Fig. 13 shows the dependence upon the difference $E_F - E(k)$ of the BHF approximation $\bar{W}_{\mathrm{BHF}}(E(k))$. In the energy range $|E_F - E(k)| < 50$ MeV, which is of physical interest, our results are quite close to those obtained by Orland and Schaeffer[7] from their dispersion relation approach, and which are represented by the long dashes in Fig. 13. The short dashes correspond to the dependence upon $E_F^{\mathrm{R}} - E^{\mathrm{R}}(k)$, Eq. (2.18), of the renormalized BHF approximation, i.e., of

$$(1-\kappa)^2 W_{\mathrm{BHF}}(E(k)). \tag{4.3}$$

We note that the renormalized approximation lies higher than the BHF approximation despite the reduction factor $(1-\kappa)^2$; this reflects the difference between the two energy scales used in the abscissa to characterize the quasiparticle state.

B. Comparison with empirical values

One may wonder to what extent the single-particle width in a finite nucleus, as measured from knockout or pickup reactions, is related to the width of a quasiparticle in infinite nuclear matter. In the case of the real part of the field, the existence of a close correspondence between the finite and infinite systems is established by the very weak dependence of the empirical depth upon mass number A. One can expect that the dependence upon A of the single-particle width is more erratic. Indeed, the width is very much influenced by the nature and by the excitation energy of the core excited states. This is particularly true for the single-particle states which lie close to the Fermi surface.[29] In Fig. 14, we have plotted versus A the width of the single-particle states which had been compiled by Jacob and Maris.[30] These plots confirm that the scatter of the empirical widths is larger for the weakly bound states ($1d$ for $A > 30$, $1p$ for $A < 20$) than for the deeply bound $1s$ states. The fairly smooth A dependence of the width of the $1s$ states suggests that they may successfully be accounted for by a nuclear matter approach. Figure 14 shows that the A dependence is fairly well reproduced by the laws which had been proposed by Hughes, Fallieros, and Goulard[31] on the one hand, namely

$$\Gamma_{1s} = 4.8A^{1/3}, \tag{4.4}$$

and by Ho-Kim[32] on the other hand, namely

$$\Gamma_{1s} = 6.3A^{1/3}. \tag{4.5}$$

Another requirement that should be fulfilled in order to be able to map nuclear matter and finite nuclei single-particle widths is that the latter should be a function of mainly one variable, namely the analog of k or of $E(k)$. Köhler[12] proposed to calculate the width of a single-particle state in a finite nucleus from the approximation

$$\Gamma = 2W(\langle k\rangle, E(\langle k\rangle)), \tag{4.6}$$

where W is computed in nuclear matter at a density equal to the mean density $\langle\rho\rangle$ felt by the hole in the finite nucleus, and where $\langle k\rangle$ is the average momentum of the hole. Köhler computed $\langle\rho\rangle$ and $\langle k\rangle$ from the independent-particle model with a harmonic oscillator potential well, and obtained striking agreement between the theoretical and empirical widths. It was pointed out in Refs. 10 and 11 that this excellent agreement was somewhat fortuitous. Indeed, it is worsened when one takes into account renormalization corrections and/or a better definition than Eq. (4.2) for the width of a quasiparticle state in nuclear matter. It should be identified with the full width at half maximum of the spectral function, as will be discussed in the next section.

Recently, Orland and Schaeffer[7] pointed out that the lifetime of a quasiparticle directly depends on the phase space available for its decay. This phase space is mainly determined by the difference $E_F - E(k)$ between the Fermi energy and the quasiparticle energy. This difference therefore seems to be a better variable than the quasiparticle momentum, to characterize the quasiparticle state. These two variables are represented in Fig. 15. Another motivation for preferring the difference $E_F - E(k)$ to $\langle k\rangle$ or to $E(k)$ is that it is more independent of the strength of the interaction, and is therefore less model dependent than k or $E(k)$. That is the reason why we adopted this difference as a variable in the preceding figures.

In Fig. 16, we plot the empirical single-particle widths versus the difference $E_F - E(k)$. The widths of the weakly bound $1d$ level show consid-

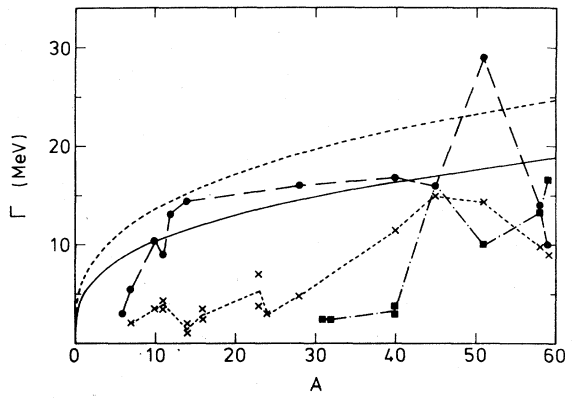

FIG. 14. Dependence upon mass number A of the empirical widths (Ref. 30) of single-particle states with quantum numbers $1s$ (full circles), $1p$ (crosses), and $1d$ (full squares). These points have been related by straight lines for visual help. The values surrounded by a circle have been extracted from Ref. 7. The smooth full curve represents Eq. (4.4) and the smooth dashed curve shows the dependence (4.5).

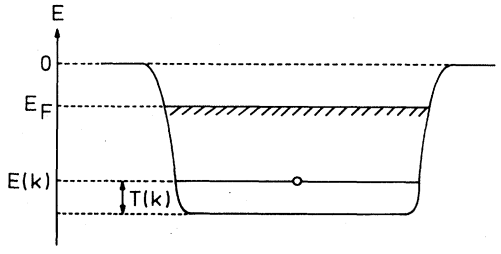

FIG. 15. Schematic representation of the Fermi energy E_F, and of the energy $E(k)$ and the kinetic energy $T(k) = k^2/2m$ of a quasiparticle state. We argue in Sec. IV B that a suitable variable for mapping nuclear matter onto finite nuclei is the difference $E_F - E(k)$.

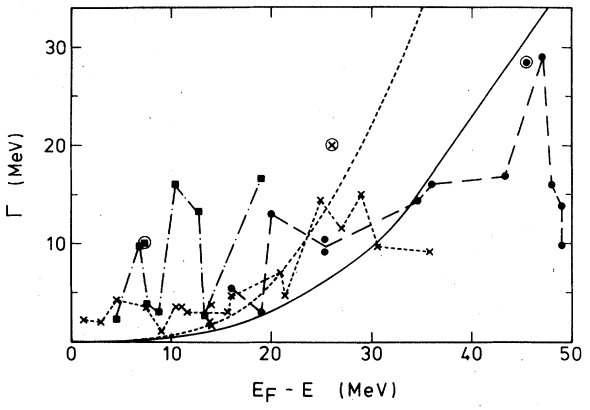

FIG. 16. Dependence upon the difference between the Fermi energy and the quasiparticle energy of the empirical widths (Ref. 30) of single-particle states with quantum numbers $1s$ (full circles), $1p$ (crosses), and $1d$ (full squares). The values surrounded by a circle are extracted from Ref. 7. We have identified the empirical value of the Fermi energy with the separation energy. The full curve shows the dependence upon $E_F - E(k)$ of the BHF approximation to the right-hand side of Eq. (4.2). The dashed curve represents the dependence upon $E_F^R - E^R(k)$ of the renormalized BHF approximation to the right-hand side of Eq. (4.2).

erable scatter; this reflects their sensitivity to finiteness effects. Hence, a nuclear matter approach is not reliable in their case. The widths of the $1p$ and $1s$ levels depend more smoothly upon $E_F - E(k)$ and, moreover, take approximately the same values. These features confirm that the widths of these single-particle states mainly depend upon the difference $E_F - E(k)$.

The comparison between the theoretical curves and the trend of the empirical data shows qualitative agreement. One might be puzzled by the appearance that the BHF approximation (full curve) yields better agreement with the data than the renormalized BHF approximation (dashed curve). However, one must keep in mind that the strength of the interaction of Hammann and Ho-Kim is too large. A rough evaluation of this overestimate can be obtained in the following way. If one multiplies $V_{(IA)}$ by a normalization factor λ, the values of $V_{(IIA)}$ and of $V_{(IIB)}$ are multiplied by λ^2. The value of λ can be adjusted in such a way that

$$\lambda V_{(IA)}(k_F) + \lambda^2[\tilde{V}_{(IIA)}(k_F) + \tilde{V}_{(IIB)}(k_F)] = -54.4 \text{ MeV} \tag{4.7}$$

for $k_F = 1.36$ fm^{-1}; see Eq. (3.3). The corresponding value of λ is equal to 0.78. The normalization correction for the width is $(0.78)^2 = 0.61$. This rough estimate indicates that with a more realistic interaction the renormalized BHF approximation to the widths would probably be at least as close to the empirical values as the BHF approximation.

V. SPECTRAL FUNCTIONS

Knockout and pickup experiments are in principle able to measure the joint probability of finding in the nuclear ground state a nucleon with momentum k and energy E.[33,34] In the case of hole states in nuclear matter, this joint probability is given by the spectral function $S_h(k;E)$ defined by

$$S_h(k;E) = \pi^{-1} \frac{W(k;E)}{\left[E - \frac{k^2}{2m} - V(k;E)\right]^2 + \frac{1}{4}[2W(k;E)]^2}. \tag{5.1}$$

In the vicinity of the quasiparticle energy, the following pole approximation is accurate[5]

$$S_h(k;E) \approx \pi^{-1} Z^2(k) \frac{\tilde{W}(k) + [E - E(k)]R(k)}{[E - E(k)]^2 + \frac{1}{4}[2Z(k)\tilde{W}(k)]^2}, \tag{5.2}$$

where $\tilde{W}(k)$ is defined by Eq. (2.4), and where

$$Z(k) = \left[1 - \frac{\partial}{\partial E} V(k;E)\right]^{-1}_{E=E(k)}, \tag{5.3}$$

$$R(k) = \left[\frac{\partial}{\partial E} W(k;E)\right]_{E=E(k)}. \tag{5.4}$$

We have used Eq. (5.2) to calculate the value of $S_h(k;E)$. The quantities $\tilde{W}(k)$, $Z(k)$, and $R(k)$ have been computed in the BHF approximation from the interaction of Hammann and Ho-Kim. In keeping with the discussion in Sec. IV B, we

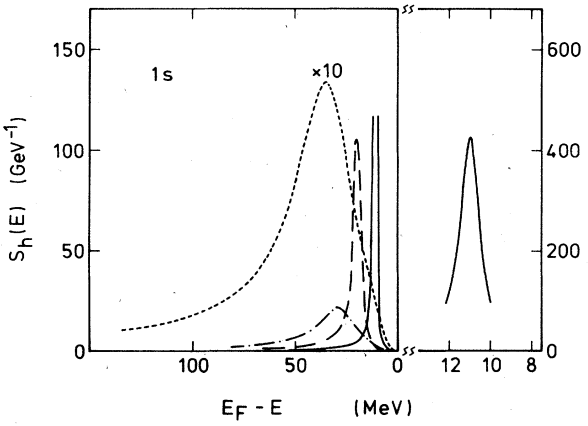

FIG. 17. Spectral functions for the $1s$ single-particle states in the nuclei ^{8}Be (full curve), ^{12}C (long dashes), ^{16}O (dash and dots), and ^{27}Al (short dashes), as calculated from the BHF approximation in nuclear matter with $k_F = 1.36$ fm^{-1}.

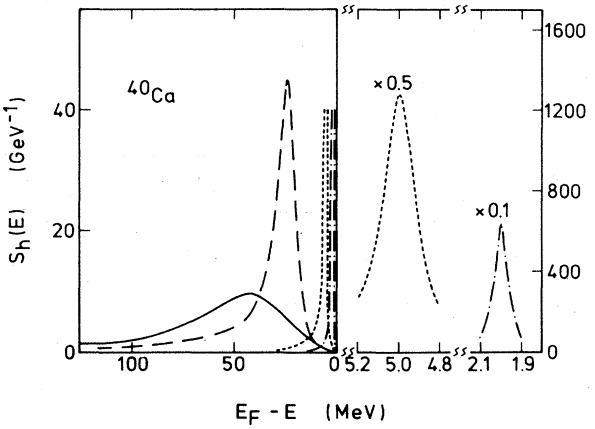

FIG. 18. Spectral functions for single-particle states in ^{40}Ca, as calculated at k_F=1.36 fm^{-1} from Eq. (5.2). The quasiparticle energy $E(k)$ in Eq. (5.2) has been adjusted to the empirical peak energy of the hole states with quantum numbers 1s (full curve), 1p (long dashes), 1d (short dashes), and 2s (dash and dots).

have adjusted the quasiparticle energy $E(k)$ in such a way that the difference $E_F - E(k)$ is equal to the empirical value.

In Fig. 17, we show the dependence upon $E_F - E$ of the spectral function $S_h(k;E)$ calculated in this way, with the energy $E(k)$ adjusted to the experimental value of the difference $E_F - E(k)$ for the 1s state in the nuclei ^{8}Be, ^{12}C, ^{16}O, and ^{27}Al. We note that the peaks are asymmetric. This is due to the term proportional to $R(k)$ in the numerator on the right-hand side of Eq. (5.2), and reflects

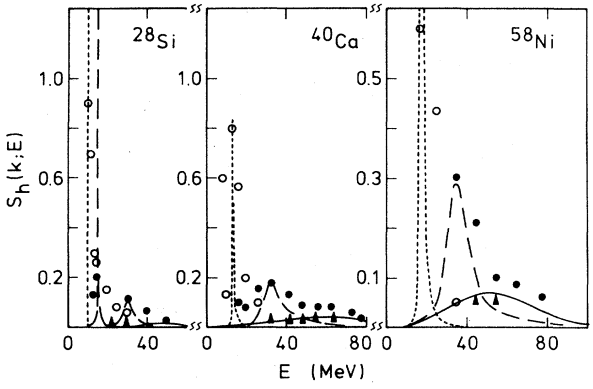

FIG. 19. Comparison between empirical strength functions (Ref. 33) and spectral functions calculated from Eq. (5.2) for k_F=1.36 fm^{-1} (ρ=0.17 nucleons/fm^3). The ordinate scale is in arbitrary units. The peak energy $E(k)$ in Eq. (5.2) has been adjusted to the empirical value for the single-particle states with quantum numbers 1s (triangles and continuous curves), 1p (full dots and long dashes), and 1d (open circles and short dashes). In the case of ^{28}Si, the two dashed curves correspond to the $1p_{3/2}$ and $1p_{1/2}$ levels, respectively.

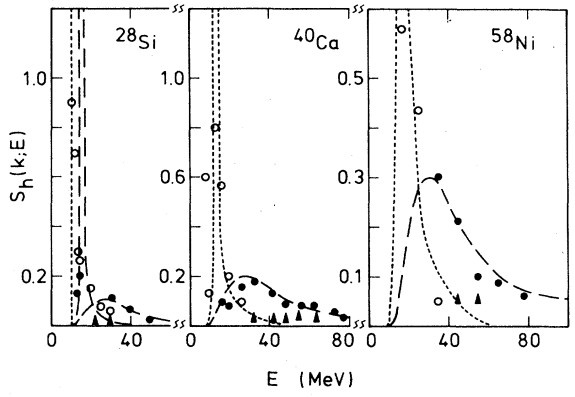

FIG. 20. Same as Fig. 19, for k_F=1.18 fm^{-1} (ρ = 0.11 nucleons/fm^3).

the fact that $S_h(k;E_F)=0$. The width of the peaks increases with increasing binding energy and, correspondingly, their height decreases.

In Fig. 18, we plot the spectral function $S_h(k;E)$, as calculated from the right-hand side of Eq. (5.2) in which we adjusted the value of $E(k)$ to the empirical energy of the 1s, 1p, 1d, and 2s hole states in ^{40}Ca; we took k_F = 1.36 fm^{-1}. These results are compared with empirical data in Fig. 19, where we also show results pertaining to ^{28}Si and ^{58}Ni. The units in the ordinate scale are arbitrary. Since the data do not directly yield the normalized spectral function, we had to attach to the theoretical curves one normalization coefficient, chosen in such a way that the height of the 1p peak is in keeping with the empirical value. We note that the agreement between the calculated and the empirical strength distributions is fair in the case of the 1s state, but that the calculated peaks are too narrow for the 1d and 1p levels. This may be partly ascribed to the fact that for these two orbits the mean nuclear density $\langle\rho\rangle$ is smaller than for the deeply bound 1s level. This is illustrated in Fig. 20 where we show the spectral functions calculated as in Fig. 19, but for the Fermi momentum k_F = 1.18 fm^{-1}.

VI. DISCUSSION

In the present paper, we studied several properties of the mean single-particle field and of hole state strength functions in nuclear matter and in finite nuclei. The input of our calculation is the semirealistic nucleon-nucleon interaction of Hammann and Ho-Kim.[9] This interaction presents two advantages over a more realistic nucleon-nucleon potential, such as Reid's for instance[35]: (a) Firstly, it is sufficiently soft for enabling one to use a perturbation expansion for the mean field, although the rate of convergence of this expansion is not fast (Sec. IIIB). Thus, we

have been able to display the contributions to the real part of the mean field of the Hartree-Fock term (Sec. III A), of the polarization graph (Sec. III B), and of the correlation graph (Sec. III C). The two latter contributions had not yet been calculated in the case of nuclear matter. We compared our results with those of Orland and Schaeffer[7] (Sec. III E), with empirical potential depths (Sec. III F), and with empirical absorptive potentials (Sec. IV B). (b) Secondly, the interaction of Hammann and Ho-Kim is of finite rank. This allows an accurate calculation of Brueckner's reaction matrix, and enabled us to investigate in detail the energy dependence of the effective mass in the Brueckner-Hartree-Fock approximation (Sec. III B), and the spectral function of hole states (Sec. V).

The interaction of Hammann and Ho-Kim suffers from the following two drawbacks: (a) It is of finite rank, i.e., is highly nonlocal. This leads to an underestimate of the effective mass in the Hartree-Fock approximation (Sec. III A), and more generally to an underestimate of the k mass $\tilde{m}(k)$ [Eq. (3.19)]. (b) The strength of the interaction of Hammann and Ho-Kim is too large. Indeed, the calculated Fermi energy is larger in absolute magnitude than the empirical value when calculated in the Brueckner-Hartree-Fock approximation.

We argued that the advantages overshadow the drawbacks. However, the latter must be kept in mind, and if possible corrected for, when comparing calculated and empirical values (Secs. III F, IV B, and V). This comparison is semiquantitatively satisfactory, if one adopts a suggestion due to Orland and Schaeffer[7] for mapping nuclear matter values onto finite nuclei properties. These authors proposed to identify in the two cases the difference between the Fermi energy and the quasiparticle energy. This prescription amounts to acribing a major role to the phase space available for the decay of the scattering state. Moreover, it largely corrects the error introduced by drawback (b) above.

This work was supported by the Institut Interuniversitaire des Sciences Nucléaires, Belgium.

[1]H. A. Bethe, Annu. Rev. Nucl. Sci. 21, 93 (1971).
[2]L. D. Landau, Sov. Phys.—JETP 8, 70 (1959).
[3]A. B. Migdal, *Theory of Finite Fermi Systems and Applications to Atomic Nuclei* (Interscience, New York, 1967).
[4]G. E. Brown, Rev. Mod. Phys. 43, 1 (1971).
[5]J. P. Jeukenne, A. Lejeune, and C. Mahaux, Phys. Rep. 25C, 83 (1976).
[6]G. F. Bertsch and T. T. S. Kuo, Nucl. Phys. A112, 204 (1968).
[7]H. Orland and R. Schaeffer, Nucl. Phys. A299, 442 (1978).
[8]R. Sartor and C. Mahaux, Phys. Rev. C 21, 1546 (1980).
[9]T. F. Hammann and Q. Ho-Kim, Nuovo Cimento 64B, 356 (1969); 14A, 633(E) (1973).
[10]R. Sartor, Nucl. Phys. A267, 29 (1976).
[11]R. Sartor, Nucl. Phys. A289, 329 (1977).
[12]H. S. Köhler, Nucl. Phys. 88, 529 (1966).
[13]G. E. Brown, J. H. Gunn, and P. Gould, Nucl. Phys. 46, 598 (1963).
[14]C. A. Engelbrecht and H. A. Weidenmüller, Nucl. Phys. A184, 385 (1972).
[15]B. Castel and K. Goeke, Phys. Lett. 82B, 160 (1979).
[16]L. Zamick, in *Common Problems in Low- and Medium-Energy Nuclear Physics*, edited by B. Castel, B. Goulard, and F. C. Khanna (Plenum, New York, 1979), p. 397.
[17]A. Lejeune and C. Mahaux, in *What do we know about the Radial Shape of Nuclei in the Ca-Region?* edited by H. Rebel, H. J. Gils, and G. Schatz (Kernforschungszentrum Karlsruhe GmBH, Karlsruhe, 1979).
[18]A. Lejuene, private communication.
[19]G. E. Brown, J. S. Dehesa, and J. Speth, Nucl. Phys. A330, 290 (1979).
[20]G. E. Brown and M. Rho, Nucl. Phys. (to be published).
[21]H. A. Bethe, G. E. Brown, J. Applegate, and J. M. Lattimer, Nucl. Phys. A324, 487 (1979).
[22]B. L. Birbrair, G. D. Alkhazov, L. P. Lapina, and V. A. Sadovnikova, Yad. Fiz. 28, 625 (1978) [Sov. J. Nucl. Phys. 28, 321 (1978)].
[23]Nguyen Van Giai, in Proceedings of the 77th Enrico Fermi Summer School (to be published); V. Bernard and Nguyen Van Giai, private communication.
[24]K. Bear and P. E. Hodgson, J. Phys. G 4, L287 (1978).
[25]J. P. Jeukenne, A. Lejeune, and C. Mahaux, Phys. Rev. C 16, 80 (1977).
[26]M. Beiner, H. Flocard, Nguyen Van Giai, and P. Quentin, Nucl. Phys. A238, 29 (1975).
[27]M. M. Giannini, G. Ricco, and A. Zucchiatti, Ann. Phys. (N.Y.) 124, 208 (1980).
[28]I. Hamamoto and P. Siemens, Nucl. Phys. A269, 199 (1976).
[29]P. Doll, G. J. Wagner, K. T. Knöpfle, and G. Mairle, Nucl. Phys. A263, 210 (1976).
[30]G. Jacob and T. A. J. Maris, Rev. Mod. Phys. 45, 6 (1973).
[31]T. A. Hughes, S. Fallieros, and B. Goulard, Nuclei and Particles 1, 93 (1971).
[32]Q. Ho-Kim, unpublished, quoted in Ref. 31.
[33]J. Mougey, M. Bernheim, A. Bussière, A. Gillebert, Phan Xuan Hô, M. Priou, D. Royer, I. Sick, and G. J. Wagner, Nucl. Phys. A262, 461 (1976).
[34]J. Mougey, J. Phys. Soc. Jpn. 44, Suppl., 420 (1978).
[35]R. V. Reid, Ann. Phys. (N.Y.) 50, 411 (1968).